

Derivation of potential profile of a dynamic quantum dot

N. Johnson,¹ G. Yamahata,¹ and A. Fujiwara^{1, a)}

NTT Basic Research Laboratories, NTT Corporation, 3-1 Morinosato Wakamiya, Atsugi, Kanagawa, 243-0198, Japan

(Dated: 8 April 2024)

We report a method to derive the potential barrier profile shape in a dynamic quantum dot and show the loading statistics, and hence accuracy of electron transfer, depend significantly on the shape of the barrier. This method takes a further step towards tunable barrier shapes, which would greatly increase the accuracy of single electron sources, allowing the single electron current to be useful for quantum sensing, quantum information and metrology. We apply our method to the case of a tunable-barrier single-electron pump, an exemplary device that shows promise as a source of hot single electron wavepackets.

Dynamic quantum dots (dQD) have been demonstrated to be able to capture single electrons with very high accuracy¹⁻⁸. Proposals for their application include roles in sensors⁹⁻¹², metrological current devices¹³⁻¹⁶, quantum information schemes¹⁷ and electron quantum optics^{18,19}. In each of these cases, the dQD provides a high-accuracy, high-fidelity source of single electron wavepackets. One promising architecture of a dQD system that can be embedded in the above mentioned proposals is the tunable-barrier single-electron pump. This is a system in which a barrier with a time varying potential creates a dQD, isolates a single electron within the dQD, and ejects the resident electron to the drain, within each cycle of the time varying potential. The forward-ejected electrons create a dc current. This out-of-equilibrium architecture is expected to be able to fulfil the criterion of becoming a realisable metrological standard at an accuracy level of 10^{82} and become a leading class of single electron source. To date, however, studies of its detailed working, which would lead to better development of this class of devices, have been empirically led. In this work we begin to remedy this by deriving the potential profile of the time-varying barrier for the first time, which determines the loading process, and hence performance of a pump or dQD. This can lead to better informed lithographic designs and operation, making the dQD system far more applicable to a wide class of single-electron based technologies.

In a dynamic quantum dot system, electrons are captured in a quantum dot (QD) by crossing a time-dependent potential barrier. In the tunable-barrier single-electron pump, the dQD is emptied by ejecting electrons over a fixed static barrier. Under the correct operating parameters, this ejection process can be made to occur with unit probability, making the accuracy of the resultant current dependent only on the loading process²⁰⁻²². The accuracy of a dQD can be defined as the fidelity of capturing a fixed given number of electrons. During the loading process, the dQD population is sensitive to tunnelling across the dynamic barrier and thermal fluctuations. Hence, understanding the dynamic barrier

potential profile at the time of loading (see Fig. 1(b)) is crucial for creating the highest accuracy devices, and establishing a high fidelity single electron source. Further, we note this characteristic cannot be derived from the single electron transistor (SET) behaviour of a device, because of the time-dependent energy scale. In an SET, the main parameters determining the threshold for conduction are the temperature and the addition energy. In a dynamical system, we counter that the role of these parameters is somewhat different because of the interplay between the thermal excitation and barrier tunnelling.

In this letter we derive the potential profile of the dQD of a tunable-barrier single-electron pump by measuring the temperature dependence of the transfer accuracy. We propose this as a general method that can be used to evaluate design critical parameters of a dQD, such as the barrier shape, charging energy, and cross-coupling between the dynamic barrier and quantum dot. All of these parameters will affect the absolute accuracy of the dQD system, and the fidelity of the system to act as a source of tunable size wavepackets^{10,18,19,23,24}. We note that whilst the model accuracy of an individual device can be evaluated straightforwardly^{2,20,22}, this value provides no information on how to improve such accuracy or its limiting parameters. Here we provide a new dimension of measurement, which we can envisage can become a central technique in leading future device design.

Figure 1(a) shows an image of a device similar to the one studied in this work. A Si-nanowire of width 10 nm is spanned by two polycrystalline-Si gates G_1 and G_2 , which have length 40 nm and separation 100 nm. They are separated from the nanowire by a thermally grown 30 nm oxide layer. When voltages V_{ent} and V_{exit} are applied to each gate G_1 and G_2 respectively, potential barriers are formed in the channel underneath the gate. A polycrystalline-Si upper gate covers the complete area in the image, to aid conduction. Because our device works predominantly using electric field confinement, we suggest our methodology and results discussed here apply equally to dQD constructed in other media^{2,22}.

V_{ent} is composed of a sinusoidal ac waveform with dc offset $V_{ent} = V_{ent}^{AC} + V_{ent}^{DC}$, whilst V_{exit} is dc only. The potential profile created by the two gates along the nanowire is sketched in Fig. 1(b). We separate the period of V_{ent}^{AC}

^{a)} akira.fujiwara.kd@hco.ntt.co.jp

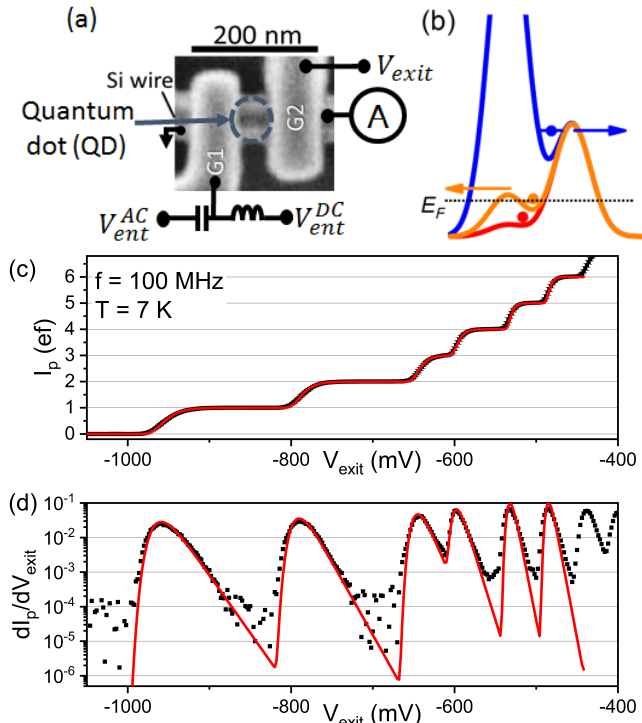


FIG. 1. (a) A silicon tunable-barrier single-electron pump equivalent to the one used in this work. Polycrystalline-Si gates G_1 and G_2 span a Si nanowire, and can be used to form potential barriers, forming a QD in between them in the case of single electron pump operation. (b) Principle of operation of the electron pump. G_1 is driven by the ac voltage V_{ent}^{AC} whilst G_2 is held static by V_{exit} . Potential profile defining the QD for three stages in the cycle of V_{ent}^{AC} . Red - initial population, orange - escape, blue - ejection. The red and orange stages together determine the loading profile. (c) Electron pump transfer current $I_p = nef$, with $n = 0$ to 6 shown here (black), and a decay cascade model fit (red). (d) Derivative dI_p/dV_{exit} , with the corresponding derivative of the decay cascade fit in red.

into three key stages of the pump cycle. In red, the dQD energy is below the Fermi energy E_F and electrons can populate the dQD. As the potential rises (orange), escape to the source occurs to leave a dQD with metastable occupation n . It is at this stage an error, defined as the occupation of any value of n other than the most probable (including $n = 0$) is most likely to occur. The loading profile is determined by these two stages. Finally, this population is frozen in as the dQD is isolated, and the potential barriers are large. Towards the maximum amplitude of V_{ent}^{AC} , the dQD is emptied (blue) and all resident electrons are ejected to the drain. This creates a dc current $I_p = nef$, with e the electronic charge and f the repetition frequency²⁵. By measuring I_p and comparing it to the expected value for perfect transfer, we measure the loss of electrons during the escape to source phase, and hence evaluate the error. We measure our device at $f = 100$ MHz, understood to be sufficiently low to allow

the loading process to occur adiabatically^{26,27}. We use current to voltage conversion of 10^{10} V/A using a Femto DDCPA-300 amplifier connected to the drain lead and I_p is measured by an HP3458A voltmeter using 10 NPLC averaging to minimise noise. The sample is mounted in a dilution refrigerator with temperature-controllable base plate in zero magnetic field²⁴.

In Fig. 1(c) we show an example trace of I_p , which shows plateaus for successive n ($n = 0$ to 6 are plotted) at temperature $T = 7$ K. In red, we plot a fit of I_p to the decay cascade model^{20,28}. This is an analytic solution to the master equation of the back tunnelling rate, and a fit is given by

$$I_p = \sum_n \exp \left(- \exp \left[-\delta_n \frac{V_{exit} - V_n}{V_{n+1} - V_n} \right] \right), \quad (1)$$

where V_n is the onset in V_{exit} for plateau of population n , and δ_n a measure of slope, and hence accuracy. Because of the appropriateness of this fit, we expect the cross-coupling between G_1 and the QD to be large²⁴, so that the QD is continuously out of equilibrium. This is an important criterion for evaluation of our method, and will produce better accuracy than those devices where the QD is in equilibrium^{21,24}.

Figure 1(d) plots the derivative dI_p/dV_{exit} for the data shown in Fig. 1(c). This distribution is representative of the population for successive n . We see the distributions are clearly asymmetric, which is a key feature of the decay cascade model and strong evidence the quantum dot potential varies in time^{20,25}. In red on Fig. 1(d) we plot the derivative of the decay cascade fit, which shows excellent agreement. We would expect non-parabolicity and shape effects to quickly cause the measured distributions of Fig. 1(d) to diverge from the fit, because the analytic solution to the decay cascade model uses a parabolic barrier in its solution of the WKB method in deriving the tunnelling rates²⁰. The excellent agreement to data of the decay cascade fit therefore allows us to clearly state that the QD potential profile, and by extension, the form of the entrance barrier created by G_1 , is parabolic²¹. This claim is strengthened by the accuracy of the fit at high n , implying a strong parabolicity to at least $n = 6$.

δ_n characterises the energy dependence of the escape rate across G_1 . It determines the slope of the riser between plateaus (see Fig. 1(c)), and hence is proportional to the flatness of the plateau, making it a valuable measure of a sample's accuracy^{2,5,20,21}. The total error rate of the pump is determined by δ_n . In the following discussion, we will examine δ_1 , the dominant source of error in pumping a single electron, to deduce the error and evaluate the device potential profile. To do this, we exploit the temperature dependence of the system. Figure 2(a) plots I_p as a function of V_{exit} , equivalent to Fig. 1(c), for successive temperatures $T = 10 - 80$ K for $n = 1$. The definition of the plateau quickly declines, implying a higher error rate with increasing T . Figure 2(b) plots δ_1 for the range of T plotted in Fig. 2(a). We identify two

regimes, the tunnelling limit, at $T < T_0$, where the dominant escape mechanism to induce an error is tunnelling across the potential barrier G_1 , and the thermal limit $T > T_0$, where the dominant mechanism of escape from the dQD is thermally activated barrier hopping^{29–31}. We define the cross-over temperature T_0 as the value of T where these rates are equal. We can express δ_1 as $\delta_1 = \left(1 + \frac{1}{g}\right) \frac{E_c}{kT^*}$, where $g = \alpha_{ent-QD} / (\alpha_{ent} - \alpha_{ent-QD})$ is a measure of the cross-coupling between the dQD and V_{ent} ($\alpha_y = eC_y/C_\Sigma$, where C_y is the capacitance from source of electric field y and C_Σ is the total capacitance to the dQD, see Fig. 3(c))²¹, k is Boltzmann's constant, and T^* is an effective temperature^{21,24}. This cross-coupling is sometimes expressed equivalently as the plunger to barrier ratio $\Delta_{ptb} = gkT_0$ ²². Then, $T^* = T_0$, $T < T_0$, and $T^* = T$, $T > T_0$ and hence the pump's best accuracy (when $T < T_0$) is determined by the tunnel barrier profile, and the charging energy E_c . We plot this dependency on Fig. 2(b) as the shaded grey line, finding good agreement for $T_0 = 17$ K. The scaled charging energy $\left(1 + \frac{1}{g}\right) E_c$ is a free parameter in this fit, and we find $\left(1 + \frac{1}{g}\right) E_c \sim 17.8$ meV, which although an overestimate of E_c , is in agreement with previous estimates^{5,10,25,32}. This suggests g is large, in agreement with the asymmetry of the population profile of Fig. 1(d)²⁴. It is very difficult to directly evaluate g , because there is no direct mapping between its value and the shape of the distribution. However, we note that $g = 0$ is a fully static quantum dot (thermal equilibrium condition) and increasing g couples the QD to V_{ent} , creating the dynamic quantum dot. Because of the asymmetry of the distributions in Fig. 1(d), we can conclude the QD is dynamic and so $g \gg 1$. We assume $g \sim 10^{24}$, and so $E_c \sim 15.9$ meV.

From δ_n , we can evaluate the lower bound of the error of the loading process, and with T_0 , we can characterise E_c . These are two critical values of merit in determining the usefulness of a single-electron wavepacket source. To begin to have control over these parameters, we need to know the form of the potential profile in the dQD and the barrier formed by G_1 . We can construct this profile from information about the temperature dependence, and T_0 . To do this, we examine I_p at fixed V_{exit} , as plotted in Fig. 3(a). Here, we plot I_p as a function of V_{exit} for successive temperatures T from 20 - 80 K, similarly to Fig. 2(a). We examine the current at the vertical cuts as marked in Fig. 3(a).

In the limit of the validity of the decay cascade model, we can equivalently express I_p as^{2,21,22,25}

$$I_p = \exp\left(-\exp\left(-\frac{\alpha V_{exit}}{kT^*} + \ln\left(\frac{\Gamma_1}{\Gamma_{inc}}\right)\right)\right), \quad (2)$$

where $\alpha = \alpha_{exit}\alpha_{ent}/\alpha_{ent-QD}$ is the relative capacitive coupling of the dQD from V_{exit} . Γ_1 is the total backtunnelling rate when the potential of the dQD crosses the Fermi level E_F of the source lead for $V_{exit} = 0$, and Γ_{inc} is a measure of the relative change in escape due

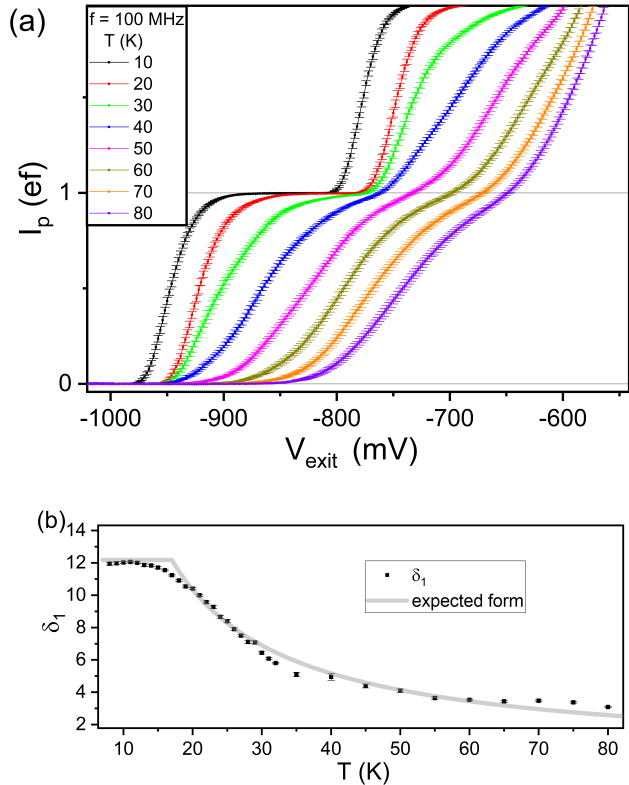


FIG. 2. (a) I_p as a function of temperature T . Traces are equivalent to those of Fig. 1(c). (b) δ_1 as extracted from a fit to the decay cascade model (see Fig. 1(c)) of the traces in (a). In grey, we mark the approximate expected relationship between δ_1 and T , finding $T_0 = 17$ K and $E_c \sim 15.9$ meV.

to the rising of the voltage V_{ent}^{AC} . For simplicity, we will assume V_{ent}^{AC} rises linearly, and assume that E_c is sufficiently large that over the temperature range studied here we only have a significant contribution from the $n = 1$ state. Then, eqn. 1 can be compared to eqn. 2 directly, up to an unknown offset in V_{exit} (this prevents us from evaluating the barrier profile directly from δ_n). This offset arises because the energy of the dQD at the time of formation is unknown.

In Fig. 3(b) we compare the exponent terms by plotting $\ln(-\ln(I_p))$ with T^{33} . We perform the fit to the data of Fig. 3(b)³⁴ as $\ln(-\ln(I_p)) = \ln(\Gamma_V/\Gamma_{inc})$ with $\Gamma_V = \Gamma_a \left(\exp\left(-\frac{\Delta}{kT}\right) + \exp\left(-\frac{\Delta}{kT_0}\right) / \left(1 + \exp\left(-\frac{\Delta}{kT_0}\right)\right)\right)$, and $\Gamma_{inc} = (\alpha_{ent} - \alpha_{ent-QD}) dV_{ent}^{AC}/dt / (kT^*)$. Here, Γ_a is the attempt frequency, Δ is the entrance barrier height at the point when the dQD level crosses E_F (see Fig. 3(c)), and we express $V_{ent}^{AC} = 2\alpha_{ent}ftV_{pp}$ with V_{pp} the peak to peak voltage of V_{ent}^{AC} . We note the most likely time for backtunnelling to occur is just after the dQD potential crosses the lead level, and hence Δ is a critical parameter in determining the backtunnelling rate. We define the successive terms in brackets for Γ_V as a thermal hopping contribution ($\exp\left(-\frac{\Delta}{kT}\right)$) and a tunnelling

contribution $\left(\exp\left(-\frac{\Delta}{kT_0}\right) / \left(1 + \exp\left(-\frac{\Delta}{kT_0}\right)\right)\right)^{24,26}$.

The fit contains two free parameters, Δ and Γ_a , which are plotted in the inset to Fig. 3(b). We expect that Δ would vary with V_{exit} linearly because of the contribution of the cross capacitance via $\alpha_{exit-QD}$, and we find this to be the case. Γ_a should be more constant over this range, because it is dependent more on the shape of the dQD potential profile, and again we find fair agreement with $\Gamma_a \sim 50$ GHz. In the inset to Fig. 3(b), the error plotted is simply the error on the fit, which incorporates the error in the measurement. We note that for $V_{exit} = -780$ mV, which lies close to the region where $n = 2$ dynamics are dominant, the deviation of Δ from a straight line is minor, as we expect the contribution from $n = 2$ to be at least one order of magnitude smaller even in this close proximity. In the fit, we have used the value of T_0 extracted from Fig. 2(b). We expect that at low temperature, the cross-over region is not well fit due to the measurement uncertainty; $\ln(-\ln(I_p)) = -6$ corresponds to $I_p/ef \sim 0.998$, which is at the limit of our experimental resolution³⁵.

In Fig. 3(c) we combine our results and sketch the form of the potential profile. On the plateau, where the sample should be tuned to find its best possible accuracy for $n = 1$, we find $\Delta \lesssim E_c$, as expected before we see the dominance of the $n = 2$ contribution that can be stably permitted for $\Delta = E_c$ (see Fig. 1(c)). We can evaluate the barrier size x_0 for a given Δ by expressing the potential due to V_{ent} as $V_{ent} = \Delta - m\omega^2 x^2/2$, with x the spatial dimension along the length of the channel. ω can be found from noting that for a parabolic potential $T_0 = \hbar\omega/2k\pi^{24}$. For our sample we derive $x_0 = 26$ nm at $V_{exit} = -780$ mV, i.e. at the point of best accuracy. This is consistent with an expected lithographic length of G_1 of ~ 40 nm.

In conclusion, we have presented a method that derives the barrier and dQD potential profile by measuring the backtunnelled current from the dQD at various temperatures. We can state our method in three key steps: (i) measure the transferred current I_p as a function of V_{exit} and fit the decay cascade model (eqn. 1) to establish parabolicity; (ii) extract the parameter δ_n as a function of temperature from the fit to evaluate absolute accuracy and identify the cross-over temperature T_0 ; and (iii) fit the measured current as a function of T at fixed V_{exit} to extract Δ , x_0 and reconstruct the barrier and dQD profile shapes.

For engineering the best possible accuracy of the dQD system, T_0 should be minimised and E_c should be maximised, which can be achieved by increasing the gate length of G_1 . Further, we suggest using a non-heterogeneous depth profile of the gate to achieve non-parabolicity in the potential shape.

This work was partly supported by JSPS KAKENHI Grant Number JP18H05258.

¹M. D. Blumenthal, B. Kaestner, L. Li, S. Giblin, T. J. B. M.

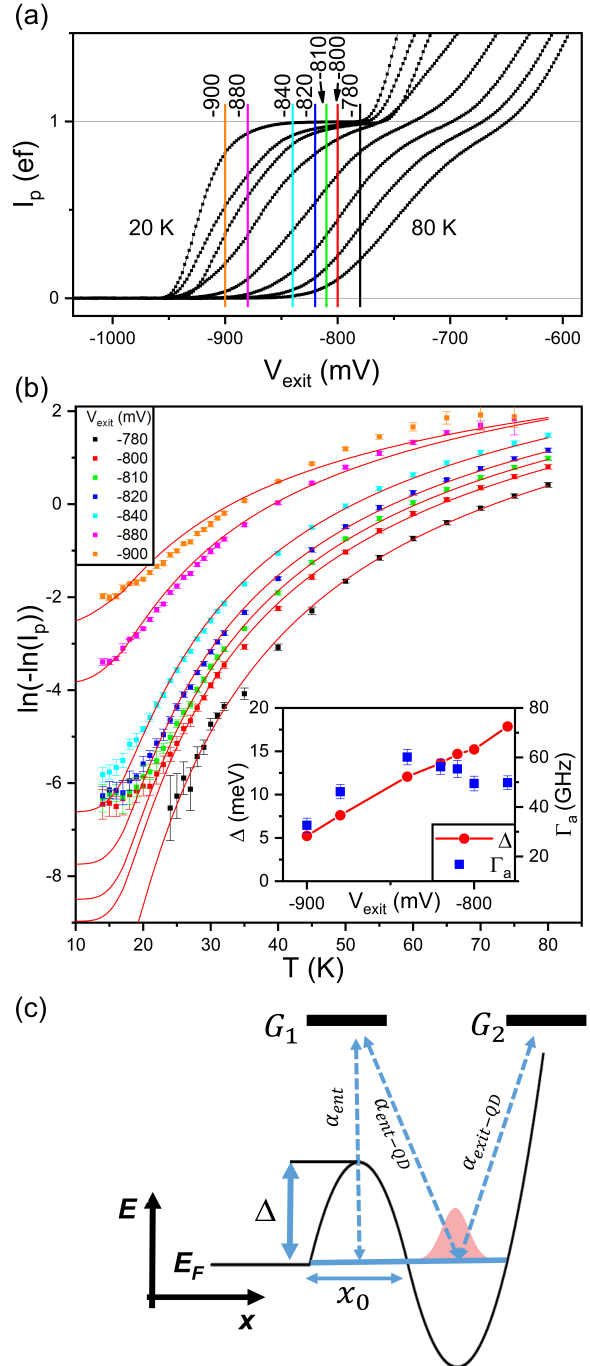


FIG. 3. (a) I_p as a function of V_{exit} for $T = 20 - 80$ K in 10 K increments (similar to Fig. 2(a)). Vertical lines indicate measurement values of V_{exit} used in the analysis of Δ in (b). (b) Evaluation of Δ by plotting $\ln(-\ln(I_p))$ with T for the values of V_{exit} indicated by the colour matched lines in (a), with a fit in red (see main text). Inset: Δ (left axis) and Γ_a (right) evaluated for each V_{exit} used in the main plot. (c) Reconstruction of the potential profile. x is a real spatial dimension along the length of the channel. The α factors are also shown.

- Janssen, M. Pepper, D. Anderson, G. Jones, and D. A. Ritchie, *Nat. Phys.* **3**, 343 (2007).
- ²S. P. Giblin, A. Fujiwara, G. Yamahata, M.-H. Bae, N. Kim, A. Rossi, M. Möttönen, and M. Kataoka, *Metrologia* **56**, 044004 (2019).
- ³S. P. Giblin, M. Kataoka, J. D. Fletcher, P. See, T. J. B. M. Janssen, J. P. Griffiths, G. A. C. Jones, I. Farrer, and D. A. Ritchie, *Nat. Commun.* **3**, 1935 (2012).
- ⁴M.-H. Bae, Y.-H. Ahn, M. Seo, Y. Chung, J. D. Fletcher, S. P. Giblin, M. Kataoka, and N. Kim, *Metrologia* **52**, 195 (2015).
- ⁵G. Yamahata, S. P. Giblin, M. Kataoka, T. Karasawa, and A. Fujiwara, *Appl. Phys. Lett.* **109**, 013101 (2016).
- ⁶R. Zhao, A. Rossi, S. P. Giblin, J. D. Fletcher, F. E. Hudson, M. Möttönen, M. Kataoka, and A. S. Dzurak, *Phys. Rev. Appl.* **8**, 044021 (2017).
- ⁷A. Rossi, T. Tantt, K. Y. Tan, I. Isakka, R. Zhao, K. W. Chan, G. C. Tettamanzi, S. Rogge, A. S. Dzurak, and M. Möttönen, *Nano Lett.* **14**, 3405 (2014).
- ⁸F. Stein, D. Drung, L. Fricke, H. Scherer, F. Hohls, C. Leicht, M. Götz, C. Krause, R. Behr, E. Pesel, K. Pierz, U. Siegner, F. J. Ahlers, and H. W. Schumacher, *Appl. Phys. Lett.* **107**, 103501 (2015).
- ⁹N. Johnson, J. D. Fletcher, D. Humphreys, P. See, J. Griffiths, G. Jones, I. Farrer, D. Ritchie, M. Pepper, T. Janssen, and M. Kataoka, *Appl. Phys. Lett.* **110**, 102105 (2017).
- ¹⁰G. Yamahata, S. Ryu, N. Johnson, H.-S. Sim, A. Fujiwara, and M. Kataoka, arXiv 1903.07802 (2019).
- ¹¹J. Waldie, P. See, V. Kashcheyevs, J. P. Griffiths, I. Farrer, G. A. C. Jones, D. A. Ritchie, T. J. B. M. Janssen, and M. Kataoka, *Phys. Rev. B* **92**, 125305 (2015).
- ¹²E. Bocquillon, F. D. Parmentier, C. Grenier, J.-M. Berroir, P. Degiovanni, D. C. Glattli, B. Plaçais, A. Cavanna, Y. Jin, and G. Fève, *Phys. Rev. Lett.* **108**, 196803 (2012).
- ¹³N. M. Zimmerman and M. W. Keller, *Meas. Sci. Tech.* **14**, 1237 (2003).
- ¹⁴S. P. Giblin, M.-H. Bae, N. Kim, Y.-H. Ahn, and M. Kataoka, *Metrologia* **54**, 299 (2017).
- ¹⁵H. Scherer and H. W. Schumacher, *Ann. Phys.* **531**, 1800371 (2019).
- ¹⁶N.-H. Kaneko, *IEEEJ Trans. Elec. Electron. Eng.* **12**, 627 (2017).
- ¹⁷C. Bäuerle, D. C. Glattli, T. Meunier, F. Portier, P. Roche, P. Roulleau, S. Takada, and X. Waintal, *Rep. Prog. Phys.* **81**, 056503 (2018).
- ¹⁸J. D. Fletcher, P. See, H. Howe, M. Pepper, S. P. Giblin, J. P. Griffiths, G. A. C. Jones, I. Farrer, D. A. Ritchie, T. J. B. M. Janssen, and M. Kataoka, *Phys. Rev. Lett.* **111**, 216807 (2013).
- ¹⁹J. D. Fletcher, N. Johnson, E. Locane, P. See, J. P. Griffiths, I. Farrer, D. A. Ritchie, P. W. Brouwer, V. Kashcheyevs, and M. Kataoka, arXiv 1901.10985 (2019).
- ²⁰V. Kashcheyevs and B. Kaestner, *Phys. Rev. Lett.* **104**, 186805 (2010).
- ²¹A. Fujiwara, G. Yamahata, and K. Nishiguchi, in *Nanoscale Silicon Devices* (CRC Press, 2016) Chap. 9.
- ²²B. Kaestner and V. Kashcheyevs, *Rep. Prog. Phys.* **78** 103901 (2015).
- ²³N. Johnson, C. Emary, S. Ryu, H.-S. Sim, P. See, J. D. Fletcher, J. P. Griffiths, G. A. C. Jones, I. Farrer, D. A. Ritchie, M. Pepper, T. J. B. M. Janssen, and M. Kataoka, *Phys. Rev. Lett.* **121**, 137703 (2018).
- ²⁴G. Yamahata, K. Nishiguchi, and A. Fujiwara, *Phys. Rev. B* **89**, 165302 (2014).
- ²⁵A. Fujiwara, K. Nishiguchi, and Y. Ono, *Appl. Phys. Lett.* **92**, 042102 (2008).
- ²⁶N. Johnson et al., In Preparation.
- ²⁷M. Kataoka, J. D. Fletcher, P. See, S. P. Giblin, T. J. B. M. Janssen, J. P. Griffiths, G. A. C. Jones, I. Farrer, and D. A. Ritchie, *Phys. Rev. Lett.* **106**, 126801 (2011).
- ²⁸B. Kaestner, V. Kashcheyevs, G. Hein, K. Pierz, U. Siegner, and H. W. Schumacher, *Appl. Phys. Lett.* **92**, 192106 (2008).
- ²⁹H. Grabert and U. Weiss, *Phys. Rev. Lett.* **53**, 1787 (1984).
- ³⁰A. O. Caldeira and A. J. Leggett, *Phys. Rev. Lett.* **46**, 211 (1981).
- ³¹P. G. Wolynes, *Phys. Rev. Lett.* **47**, 968 (1981).
- ³²G. Yamahata, K. Nishiguchi, and A. Fujiwara, *Appl. Phys. Lett.* **98**, 222104 (2011).
- ³³We note there was a discontinuity seen around $T = 32$ K, arising from a thermal cycle occurring to the device. On remeasuring the device, it was found δ_1 was unchanged (ensuring consistency and generality of results) but the position in V_{exit} had slightly shifted by 14 mV. This has been accounted for in this analysis by offsetting curves for $T < 32$ K. Note that the curves of Figs. 2(a) and 3(a) are also offset.
- ³⁴In the analysis of Fig. 3(b), low temperature data was excluded from the fit owing to instability of the curve position in V_{exit} , which we speculate is due to a changing channel conductance³⁶.
- ³⁵The error bars plotted in Fig. 3(b) are the Type A (statistical) uncertainty, and these are used in the fit. The limit of our measurement resolution, and hence Type A uncertainty, is approximately 0.2 pA, which corresponds to $\ln(-\ln(I_p)) \sim 6$, and points below this are not used in the fit. To show the crossover to the tunnelling regime, we extend the fit curve in to this region.
- ³⁶A. Fujiwara, Y. Takahashi, H. Namatsu, K. Kurihara, and K. Murase, *Jpn. J. Appl. Phys.* **37**, 3257 (1998).